



Version: 3.2

A Search For B_s^0 Oscillations Using $B_s^0 \rightarrow D_s \mu X$ ($D_s \rightarrow K_S^0 K$) Decays

The DØ Collaboration
URL <http://www-d0.fnal.gov>
(Dated: October 24, 2006)

We perform a search for B_s^0 oscillations in a sample of 593 tagged $B_s^0 \rightarrow D_s \mu X$ ($D_s \rightarrow K_S^0 K$) events corresponding to $\sim 1.2 \text{ fb}^{-1}$ of data collected by the DØ detector. Using opposite-side tagging to determine the initial-state flavor and an unbinned likelihood fit method, we obtain a 95% confidence level limit on the oscillation frequency $\Delta m_s > 1.09 \text{ ps}^{-1}$ and a sensitivity of 1.90 ps^{-1} .

Preliminary Results for Fall 2006 Conferences

I. INTRODUCTION

Neutral B_d^0 and B_s^0 mesons mix with their antiparticles leading to oscillations between the flavor eigenstates. $B_d^0 - \bar{B}_d^0$ oscillations have been observed first by the UA1 collaboration [1] in a mixture of B_d^0 and B_s^0 mesons and then by the ARGUS collaboration [2] in B_d^0 mesons. The frequency of B_s^0 oscillations, Δm_s , can be combined with the well-known frequency of B_d^0 oscillations, $\Delta m_d = 0.502 \pm 0.007 \text{ ps}^{-1}$ [3], to reduce the uncertainty on the CKM matrix element $|V_{td}|$ through the formula [4],

$$\frac{\Delta m_s}{\Delta m_d} = \frac{m(B_s^0)}{m(B_d^0)} \xi^2 \left| \frac{V_{ts}}{V_{td}} \right|^2, \quad (1)$$

where ξ is estimated from Lattice QCD calculations to be $1.15 \pm 0.05_{-0.00}^{+0.12}$ [3].

Recently, DØ has measured the world's first two-sided bound on Δm_s of $17.0 < \Delta m_s < 21.0 \text{ ps}^{-1}$ at the 90% C.L with a most probable value of $\Delta m_s = 19 \text{ ps}^{-1}$ [5]. CDF later confirmed the bound with a measurement of $\Delta m_s = 17.31_{-0.18}^{+0.33} (\text{stat.}) \pm 0.07 (\text{sys}) \text{ ps}^{-1}$ [6].

The two-sided bound on Δm_s described in Ref. [5] used the semileptonic decay mode $B_s^0 \rightarrow D_s^- \mu^+ X$ ($D_s^- \rightarrow \phi \pi^-$). Subsequent analyses added the modes $B_s^0 \rightarrow D_s^- \mu^+ X$ ($D_s^- \rightarrow K^*(892)^0 K^-$) and $B_s^0 \rightarrow D_s^- e^+ X$ ($D_s^- \rightarrow \phi \pi^-$) for an updated result [7]. This analysis intends to add the channel $B_s^0 \rightarrow D_s^- \mu^+ X$ ($D_s^- \rightarrow K_S^0 K^-$) to improve the sensitivity of the overall combined B_s^0 mixing result. The relatively smaller statistics of this channel results in a poorer sensitivity than the other individual channels, but will still contribute in the combination; this result is not intended as a “stand-alone” result.

II. DETECTOR DESCRIPTION

The DØ detector is described elsewhere [8]. The following elements of the DØ detector are essential for this analysis:

- a magnetic central-tracking system, which consists of a silicon microstrip tracker (SMT) and a central fiber tracker (CFT), both located within a 2-T superconducting solenoidal magnet;
- a liquid-argon/uranium calorimeter; and
- a muon system located beyond the calorimeter.

The SMT has 800,000 individual strips, with typical pitch of $50 - 80 \mu\text{m}$, and a design optimized for tracking and vertexing capability at $|\eta| < 3$, where $\eta = -\ln(\tan(\theta/2))$ and θ is the polar angle. The CFT has eight thin coaxial barrels, each supporting two doublets of overlapping scintillating fibers of 0.835 mm diameter, one doublet being parallel to the collision axis, and the other alternating by $\pm 3^\circ$ relative to the axis. The resolution of the impact parameter with respect to the collision point is approximately $20 \mu\text{m}$ for 5 GeV/c tracks.

The three components of the liquid-argon/uranium calorimeter are housed in separate cryostats. A central section, lying outside the tracking system, covers up to $|\eta| = 1.1$. Two end calorimeters extend the coverage to $|\eta| \approx 4$.

The muon system consists of a layer of tracking detectors and scintillation trigger counters inside a 1.8 T iron toroid, followed by two additional layers outside the toroid. Tracking at $|\eta| < 1$ relies on 10 cm wide drift tubes, while 1 cm mini-drift tubes are used at $1 < |\eta| < 2$.

III. DATA SAMPLE

This analysis used a $B_s^0 \rightarrow D_s^- \mu^+ \nu X$, $D_s^- \rightarrow K_S^0 K^-$ data sample selected through an offline filter from all data accumulated by the DØ detector during the period from April 2002 to February 2006, also referred to as Run 2a. No explicit trigger requirement was required, although most of the data was collected by single muon triggers. The selections for the offline filter are described below. Charge conjugated states are implied throughout.

The primary vertex position in the transverse plane was determined on an event-by-event basis by requiring the tracks in the event to come from a common collision point that is constrained by the mean beam-spot position calculated on a run-by-run basis.

We begin the reconstruction of this mode by searching for a muon required to have $p_T > 2 \text{ GeV}/c$ and $|\vec{p}| > 3 \text{ GeV}/c$, to have at least one hit each in the CFT and SMT, and to have measurements in at least two layers of the muon chambers.

The K_S^0 candidate was constructed from two tracks of opposite charge sharing the same primary vertex as the muon, each having at least 4 hits in the tracking detectors, two of which must be in the CFT. Cuts were applied on different mass hypotheses assigned to the tracks: for the two-pion mass hypothesis $M(\pi_1, \pi_2)$, events were required to have $460 < M(\pi_1, \pi_2) < 525$ MeV/ c^2 , and for the two-electron mass hypothesis $M(e_1, e_2)$, events were required to have $M(e_1, e_2) > 25$ MeV/ c^2 to reduce the contribution from photon conversions. The combined significance of the transverse and the longitudinal impact parameter projection with respect to the primary vertex,

$\epsilon_{sig} = \sqrt{(\epsilon_T/\sigma(\epsilon_T))^2 + (\epsilon_L/\sigma(\epsilon_L))^2}$ was required to be greater than 3 for each track. Events that had $\epsilon_{sig} < 4$ for both tracks were also rejected. The transverse decay length of the K_S^0 , $d_T(K_S^0)$, was required to satisfy $d_T(K_S^0) > 0.3$ cm, the p_T of the K_S^0 was required to satisfy $p_T(K_S^0) > 650$ MeV/ c , and the K_S^0 was constrained to its nominal mass [3].

All charged particles in the event were clustered into jets using the DURHAM clustering algorithm [9] with the p_T cutoff parameter set at 15 GeV/ c [10]. The D_s^- candidate was constructed by combining the K_S^0 candidate with a third track required to be in the same jet as the muon and having a charge opposite to that of the muon. The track was required to have hits in the SMT and CFT, $p_T > 1.5$ GeV/ c , and $\epsilon_{sig} > 2$. The third track and the K_S^0 candidate were required to form a common D_s^- vertex with $\chi_D^2 < 16$ for the vertex fit. The vertexing algorithm is described in detail in Ref. [11]. The distance d_T^D between the primary and D_s^- vertices in the transverse plane was required to exceed 4 standard deviations, that is $d_T^D/\sigma(d_T^D) > 4$. The angle α_T^D between the momentum of the D_s^- candidate and the direction from the primary to the D_s^- vertex in the transverse plane was required to be $\cos(\alpha_T^D) > 0.9$;

The tracks of the muon and D_s^- candidate were required to produce a common B_s^0 vertex with $\chi_B^2 < 9$ for the vertex fit. The mass of the $(\mu^+ D_s^-)$ was required to be in the range $2.6 < m(\mu D_s) < 5.4$ GeV/ c^2 . The transverse decay length of the B_s^0 hadron, d_T^B , was defined as the distance in the transverse plane between the primary vertex and the vertex produced by the muon and D_s^- meson. If the distance d_T^B exceeded $4 \cdot \sigma(d_T^B)$, the angle α_T^B between the B_s^0 momentum and the direction from the B_s^0 vertex in the transverse plane was required to satisfy the condition $\cos(\alpha_T^B) > 0.95$. The distance d_T^B was allowed to be greater than d_T^D , provided the distance between the B_s^0 and D_s^- vertices, d_T^{BD} , was less than $2 \cdot \sigma(d_T^{BD})$. The isolation, defined as $Iso = p(\mu D_s)/(p(\mu D_s) + \sum p_i)$ where $\sum p_i$ is taken over all charged particles in the cone $\Delta R = \sqrt{(\Delta\phi)^2 + (\Delta\eta)^2} < 0.5$ and $\Delta\eta(\phi)$ is the pseudorapidity (azimuthal angle) with respect to the μD_s direction, was required to be greater than 0.3.

The final event samples were then selected using a Likelihood Ratio Method, described below.

A. Likelihood Ratio Method

We choose a set of discriminating variables x_1, \dots, x_n for each event and construct probability density functions for signal, $f^s(x_i)$, and background, $f^b(x_i)$. We then define a combined selection variable y as,

$$y = \prod_{i=1}^n y_i; \quad y_i = \frac{f_i^b(x_i)}{f_i^s(x_i)}. \quad (2)$$

In case a variable x_i cannot be constructed for a particular event, we set the corresponding y_i to 1. We select signal events by applying a cut on the combined variable, $y < y_0$ [11].

The following discriminating variables were used in the construction of the likelihood ratio probability density functions (*pdf*'s):

- $p_T(K)$;
- $p_T(K_S^0)$;
- the transverse decay length of the K_S^0 ;
- $m(\pi_1, \pi_2)$ of the K_S^0 candidate;
- the χ^2 of the D_s^- vertex fit;
- the isolation of the B as defined in Sec. III; and
- $m(\mu D_s)$.

The probability density functions were constructed using data events. We define signal (S) and background (B) regions as:

$$\begin{aligned} S &: 1.90 < M(D_s^-) < 2.02 \text{ GeV}/c^2, \quad q_\mu \cdot q_K < 0 \text{ ("opposite-sign")}; \\ B &: 1.90 < M(D_s^-) < 2.02 \text{ GeV}/c^2, \quad q_\mu \cdot q_K > 0 \text{ ("same-sign")}. \end{aligned}$$

Note that these mass region definitions arise from an estimate of the 3σ D_s signal region. The signal probability density function was constructed by subtracting the distributions of events in region B from the distribution of events in region S .

The final cut on the combined variable $\log_{10} y < -0.08$ was selected by maximizing $S/\sqrt{S+B}$. In Fig. 1 we overlay the mass spectrum before and after the likelihood ratio selection is applied. Using techniques described in Sec. III B, we estimate that the signal to background ratio in the 3σ region around the D_s signal improves from $S/B = 0.06$ to $S/B = 0.17$ after the application of likelihood ratio selections.

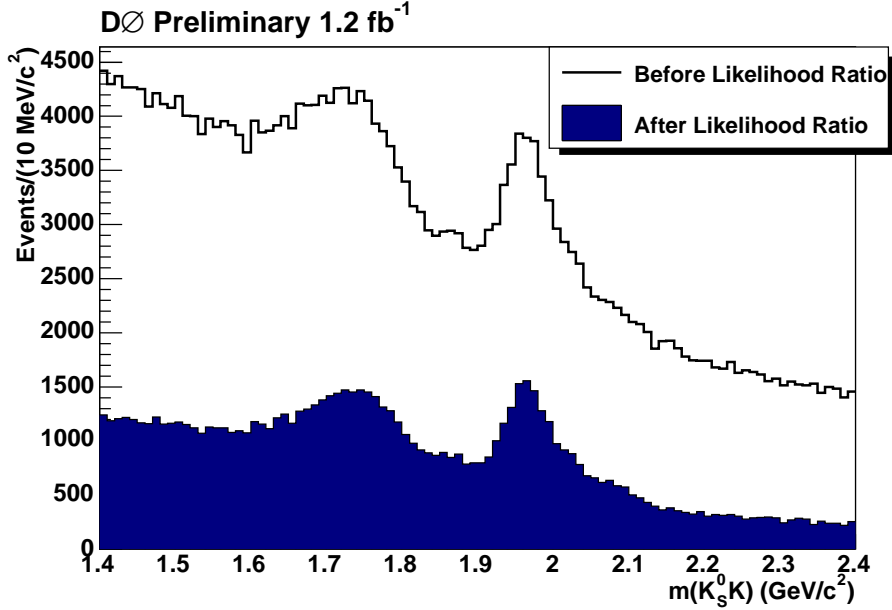


FIG. 1: Mass spectrum for $m(K_S^0 K)$ before and after likelihood ratio selections. The dominant channels contributing to the left peak are $D^{(0,+,*)} \rightarrow K_S^0 \pi^- X$ decays where some neutral particle (such as π^0 or γ) is not reconstructed. The higher mass peak contains contributions from $D_s^- \rightarrow K_S^0 K^-$, $D^- \rightarrow K_S^0 \pi^-$, and $\Lambda_c^- \rightarrow K_S^0 \bar{p}$.

B. Mass Fitting Procedure

The mass spectrum shown in Fig. 1 contains contributions from modes other than the $D_s^- \rightarrow K_S^0 K^-$ channel. The main contributions to the spectrum are listed below:

1. $D_s^- \rightarrow K_S^0 K^-$;
2. $D^- \rightarrow K_S^0 \pi^-$;
3. $D^- \rightarrow K_S^0 K^-$, which we refer to as the *Cabbibo-suppressed* mode;
4. $\Lambda_c^- \rightarrow K_S^0 \bar{p}$;
5. $D^{(0,-,*)} \rightarrow K_S^0 \pi^- X$, which we refer to as the *low-mass* mode.

We have developed an unbinned likelihood technique to separate these kinematic reflections which we describe below.

Consider a decay $X \rightarrow K_S^0 + \text{track}$, where the X can be D_s^- , D^- , or Λ_c^- . Let the track be identified as a K . For the $D^-(\Lambda_c^-)$ system this would be a misassignment of the $\pi(p)$. The mass of the $K_S^0 + \text{track}$ system is then:

$$\mathcal{M}_{mis}^2 = M_X^2 + M_K^2 - M_{trk}^2 + 2E_{K_S} E_K - 2E_{K_S} E_{trk}. \quad (3)$$

We can Taylor expand the relativistic energy in M/p , and under the assumption that $M_{K_S} \ll p_{K_S}$ we then have:

$$\mathcal{M}_{mis}^2(\lambda) = M_X^2 + \left(\frac{2}{1-\lambda} \right) (M_K^2 - M_{trk}^2), \quad (4)$$

where $\lambda = (p_{K_S} - p_{trk}) / (p_{K_S} + p_{trk})$ is the momentum asymmetry.

We can then insert a kinematic term in the likelihood as follows:

$$\mathcal{L}_i^{mass} = P_i(\lambda) \cdot \frac{1}{\sigma\sqrt{2\pi}} \exp \left[-\frac{1}{2} \left(\frac{M_{measured}(K_S K) - \mathcal{M}_i(\lambda)}{\sigma} \right)^2 \right], \quad (5)$$

where the i represents the various modes, $P_i(\lambda)$ are the distributions obtained from Monte Carlo, and $\mathcal{M}_i(\lambda)$ is Eqn. 4 for the D^- and Λ_c^- modes. The mass of the D_s^- and Cabbibo-suppressed mode do not depend on λ and therefore the likelihoods for them are simply taken as double Gaussians in mass. We use a bifurcated Gaussian in mass to model the low-mass peak.

The functions $P_i(\lambda)$ are formed by fitting polynomials to Monte Carlo distributions of λ . The function for the low mass peak, $P_{low}(\lambda)$, is constructed using information from $D^- \rightarrow K_S^0 \pi^- \pi^0$ Monte Carlo.

Because the mass of the proton from $\Lambda_c^- \rightarrow K_S^0 \bar{p}$ decays is large compared to the pion mass, the Taylor expansion implicit in Eqn. 4 does not work as well as it does for the $D^- \rightarrow K_S^0 \pi^-$ mode. We find that we have to modify Eqn. 4 by adding two ad-hoc correction terms:

$$\mathcal{M}^2(\lambda) = M_X^2 + \left(\frac{2}{1-\lambda} \right) (M_K^2 - M_{trk}^2) + a \cdot \frac{1-\lambda}{1+\lambda} + b \quad (6)$$

for the Λ_c^- mode. We fit for these two terms in Λ_c^- Monte Carlo, fixing $m(\Lambda_c^-)$ to the value obtained from fitting the $m(K_S^0 \bar{p})$ spectrum. We obtain $a = 0.1627 \pm 0.0035$ and $b = 0.1196 \pm 0.0035$.

The total number of D_s^- candidates obtained from this procedure is 2603 ± 110 (stat.) while the number of $D^- \rightarrow K_S^0 \pi^-$ candidates is 4481 ± 106 (stat.) as seen in Fig. 2. There are 593 ± 67 (stat.) B_s^0 candidates with an identified initial-state flavor as described in Sec. IV (see Fig. 3).

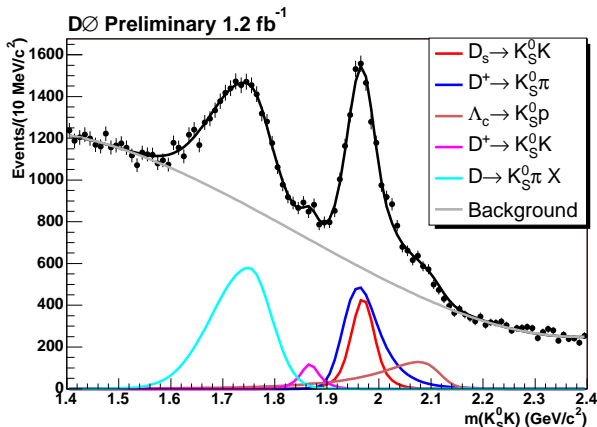


FIG. 2: $M(K_S^0 K)$ invariant mass distribution for the untagged data sample. The colored lines correspond to mass fit projections using the unbinned likelihood mass fitting procedure described in Sec. III B. The background is modelled as a third-order Chebyshev polynomial.

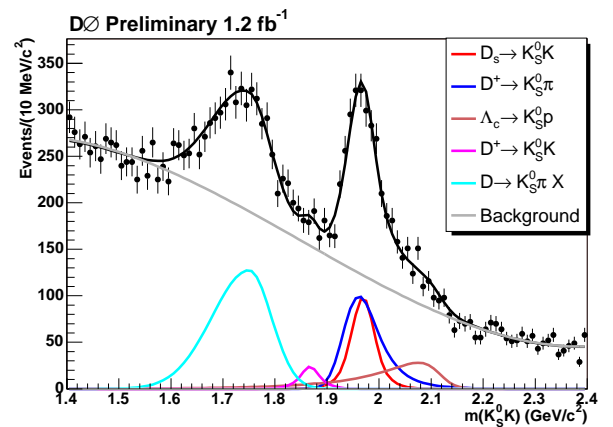


FIG. 3: $M(K_S^0 K)$ invariant mass distribution for the flavor-tagged data sample. The colored lines correspond to mass fit projections using the unbinned likelihood mass fitting procedure described in Sec. III B. The background is modelled as a third-order Chebyshev polynomial.

IV. INITIAL STATE FLAVOR TAGGING

The opposite-side initial-state flavor tagger used in this analysis is described in detail in Ref. [12]. Here we present a brief overview of the relevant tagging concepts and variables.

Opposite-side tagging (OST) of the initial flavor of the B_s^0 meson exploits the fact that in $b\bar{b}$ pair production two b -flavored hadrons are always produced. By identifying the flavor of the b hadron on the opposite side of the event from the reconstructed B_s^0 meson, we may therefore infer its flavor at the time of production. Purity, dilution, and tagging efficiency are the three important parameters used to describe the tagging performance. The purity of the tagging method is defined as $\eta_s = N_{correctly\ tagged\ events} / N_{total\ tagged\ events}$. The dilution is related to the purity by the formula $\mathcal{D} = 2\eta_s - 1$. Finally, the tagging efficiency is defined as $\epsilon = N_{total\ tagged\ events} / N_{total\ events}$.

Ref. [12] describes a measurement of the B_d^0 oscillation frequency and a determination of the dilution for the B_d^0 and B^+ samples. In that study, the independence of the OST on the flavor of the reconstructed B meson is verified, allowing us to use those results on the B_s^0 sample. Each tagged B candidate is characterized by the variable d_{pr} that gives a prediction of the dilution for that candidate using the formulas

$$\begin{aligned}\mathcal{D}(d_{pr})|_{d_{pr}<0.6} &= 0.457 \cdot |d_{pr}| + 2.349 \cdot |d_{pr}|^2 - 2.498 \cdot |d_{pr}|^3, \\ \mathcal{D}(d_{pr})|_{d_{pr}>0.6} &= 0.6.\end{aligned}\quad (7)$$

Another parameterization of $\mathcal{D}(d_{pr})$ was used to estimate the systematic uncertainty due to the dilution parameterization:

$$\mathcal{D}(d_{pr}) = \frac{0.6}{1 + \exp\left(-\frac{d_{pr}-0.312}{0.108}\right)}.\quad (8)$$

V. EXPERIMENTAL OBSERVABLES

The proper lifetime of the B_s^0 meson, $c\tau_{B_s^0}$, for semileptonic decays can be written as

$$c\tau_{B_s^0} = x^M \cdot K, \quad \text{where } x^M = \left[\frac{\mathbf{d}_T^{\mathbf{B}} \cdot \mathbf{p}_T^{\mu D_s^-}}{(p_T^{\mu D_s^-})^2} \right] \cdot cM_B.\quad (9)$$

x^M is the *visible proper decay length*, or VPDL, and K is the correction factor, also called the K factor. Semileptonic B decays necessarily have an undetected neutrino present in the decay chain, making a precise determination of the kinematics for the B meson impossible. In addition, other neutral or non-reconstructed charged particles can be present in the decay chain of the B meson. This leads to a bias towards smaller values of the B momentum, which is calculated using the reconstructed particles. A common practice to correct this bias is to scale the measured momentum of the B candidate by a K factor, which takes into account the effects of the neutrino and other lost or non-reconstructed particles. For this analysis, the K factor was defined as

$$K = p_T(\mu^+ D_s^-) / p_T(B_s^0),\quad (10)$$

where p_T denotes the absolute value of the transverse momentum. The K -factor distributions used to correct the data were obtained from Monte Carlo (MC) simulations.

VI. FITTING PROCEDURE

The likelihood for an event to arise from a specific source in the sample depends on x^M , its error (σ_{x^M}), the mass of the D_s^- meson candidate (m), the momentum asymmetry λ as defined in Sec. III B, the predicted dilution (d_{pr}), and the selection variable y as defined in Sec. III A. All of these quantities are known on an event-by-event basis. The *pdf* for each source can be expressed by the following formula:

$$\mathcal{P}_i = P_i^{x^M}(x^M, \sigma_{x^M}, d_{pr}) P_i^m(m, \lambda) P_i^{\sigma_{x^M}} P_i^{d_{pr}} P_i^y.\quad (11)$$

The VPDL *pdf* $P_i^{x^M}(x^M, \sigma_{x^M}, d_{pr})$ represents a conditional probability and therefore should be multiplied by $P_i^{\sigma_{x^M}}$ and $P_i^{d_{pr}}$ to have a joint *pdf* (see the ‘‘Probability’’ section in the PDG [3]).

The sources considered for the entire $K_S^0 K$ mass region ($1.4 < m(K_S^0 K) < 2.4$ GeV/ c^2) are the same as those enumerated in the beginning of Sec. III B in addition to a combinatorial background component. The total *pdf* for the j^{th} B candidate therefore has the form:

$$\begin{aligned}\mathcal{P}_j &= Fr_{D_s} \mathcal{P}_{D_s} + Fr_{D^+} \mathcal{P}_{D^+} + 0.13 \cdot Fr_{D^+} \mathcal{P}_{Cabbibo} + Fr_{\Lambda} \mathcal{P}_{\Lambda} + Fr_{low} \mathcal{P}_{low} + \\ &\quad (1 - Fr_{D_s} - Fr_{D^+} - 0.13 \cdot Fr_{D^+} - Fr_{\Lambda} - Fr_{low}) \mathcal{P}_{bg}.\end{aligned}\quad (12)$$

The fractions Fr_{D_s} , Fr_{D^+} , Fr_{Λ} , Fr_{low} are determined from a fit to the total tagged sample (see Fig. 3). Note that the multiplicative factor 0.13 is determined by comparing Monte Carlo efficiencies for the $D^+ \rightarrow K_S^0 K$ and $D^+ \rightarrow K_S^0 \pi$ channels.

We perform a log-likelihood minimization of

$$\mathcal{L} = -2 \sum_{j=1}^{N_{events}} \ln F_j \quad (13)$$

using MINUIT [13].

The *pdfs* for the VPDL uncertainty ($P_i^{\sigma_{x^M}}$), mass (P_i^m), dilution ($P_i^{d_{pr}}$), and selection variable y (P_i^y) were taken from experimental data. The signal *pdfs* were also used for all the peaking components listed in Sec. III B. The dependence of the background slope on VPDL was also taken into account.

A. pdf for the μD_s Signal

The μD_s sample is composed mostly of B_s^0 mesons with some contributions from B_u and B_d mesons. Different species of B mesons behave differently with respect to oscillations. Neutral B_d^0 and B_s^0 mesons do oscillate (with different frequencies) while charged B_u mesons do not.

The data sample is divided into non-oscillated and oscillated subsamples as determined by the flavor tagging. For a given type of B_q hadron, where $q = \{d, u, s\}$, the distribution of the visible proper decay length x for non-oscillated and oscillated cases (p^{nos} and p^{osc}) is given by:

$$p_s^{nos}(x, K, d_{pr}) = \frac{K}{c\tau_{B_s}} \exp\left(-\frac{Kx}{c\tau_{B_s}}\right) \cdot 0.5 \cdot (1 + \mathcal{D}(d_{pr}) \cos(\Delta m_s \cdot Kx/c)), \quad (14)$$

$$p_s^{osc}(x, K, d_{pr}) = \frac{K}{c\tau_{B_s}} \exp\left(-\frac{Kx}{c\tau_{B_s}}\right) \cdot 0.5 \cdot (1 - \mathcal{D}(d_{pr}) \cos(\Delta m_s \cdot Kx/c)), \quad (15)$$

$$p_{D_s D_s}^{osc}(x, K) = \frac{K}{c\tau_{B_s}} \exp\left(-\frac{Kx}{c\tau_{B_s}}\right) \cdot 0.5, \quad (16)$$

$$p_{D_s D_s}^{nos}(x, K) = \frac{K}{c\tau_{B_s}} \exp\left(-\frac{Kx}{c\tau_{B_s}}\right) \cdot 0.5, \quad (17)$$

$$p_u^{nos}(x, K, d_{pr}) = \frac{K}{c\tau_{B_u}} \exp\left(-\frac{Kx}{c\tau_{B_u}}\right) \cdot 0.5 \cdot (1 - \mathcal{D}(d_{pr})), \quad (18)$$

$$p_u^{osc}(x, K, d_{pr}) = \frac{K}{c\tau_{B_u}} \exp\left(-\frac{Kx}{c\tau_{B_u}}\right) \cdot 0.5 \cdot (1 + \mathcal{D}(d_{pr})), \quad (19)$$

$$p_d^{nos}(x, K, d_{pr}) = \frac{K}{c\tau_{B_d}} \exp\left(-\frac{Kx}{c\tau_{B_d}}\right) \cdot 0.5 \cdot (1 - \mathcal{D}(d_{pr}) \cos(\Delta m_d \cdot Kx/c)), \quad (20)$$

$$p_d^{osc}(x, K, d_{pr}) = \frac{K}{c\tau_{B_d}} \exp\left(-\frac{Kx}{c\tau_{B_d}}\right) \cdot 0.5 \cdot (1 + \mathcal{D}(d_{pr}) \cos(\Delta m_d \cdot Kx/c)), \quad (21)$$

Here τ is the lifetime of the B hadron and or b baryon. Note that there is a sign swap in Eqns. 18–21 with respect to Eqn. 14 and Eqn. 15 due to the anti-correlation of muon charge for $B \rightarrow DD_s$; $D \rightarrow \mu X$ processes.

The translation to the measured VPDL, x^M is achieved by a convolution of the K factors and resolution functions as specified below.

$$P_j^{osc, nos}(x^M, \sigma_{x^M}, d_{pr}) = \quad (22)$$

$$\int_{K_{min}}^{K_{max}} dK D_j(K) \cdot \frac{Eff_j(x^M)}{N_j(K, \sigma_{x^M}, d_{pr})} \int_0^\infty dx G(x - x^M, \sigma_{x^M}) \cdot p_j^{osc, nos}(x, K, d_{pr}). \quad (23)$$

$$\text{Here } G(x - x^M, \sigma_{x^M}) = \frac{1}{\sqrt{2\pi}\sigma_{x^M}} \exp\left(-\frac{(x - x^M)^2}{2\sigma_{x^M}^2}\right) \quad (24)$$

is the detector resolution of the VPDL and $Eff_j(x)$ is the reconstruction efficiency for a given decay channel j of this type of B meson as a function of VPDL. The function $D_j(K)$ gives the normalized distribution of the K factor in a given channel j . The normalization factor N_j is calculated by integration over the entire VPDL region:

$$N_j(K, \sigma_{x^M}, d_{pr}) = \frac{1}{2} \int_{-\infty}^{\infty} dx^M Eff_j(x^M) \int_0^{\infty} dx G(x - x^M, \sigma_{x^M}) \cdot (p_j^{osc}(x, K, d_{pr}) + p_j^{nos}(x, K, d_{pr})). \quad (25)$$

The total VPDL *pdf* for the μD_s signal is a sum of all the contributions which give the D_s mass peak:

$$P_{\mu D_s}^{osc, nos}(x^M, \sigma_{x^M}, d_{pr}) = \sum_j SC_j \cdot P_j^{osc, nos}(x^M, \sigma_{x^M}, d_{pr}) \times (1 - Fr_{c\bar{c}}) + Fr_{c\bar{c}} \cdot P_{c\bar{c}}^{osc, nos}(x^M). \quad (26)$$

The sum \sum_j is taken over all decay channels that yield a $\mu^+ D_s^-$ final state and the SC_j is the sample composition for a given channel j as determined using Monte Carlo reconstruction efficiencies and branching ratios (see Sec. VII). In addition to the long-lived $\mu^+ D_s^-$ candidates from B meson decays, there is a contribution, with fraction $\mathcal{F}_{c\bar{c}}$, of “peaking background”, which consists of combinations of D_s^- mesons and muons originating from different c or b quarks. Direct c production gives the largest contribution to this background and, therefore, the function $P_{c\bar{c}}^{osc, nos}(x^M)$ was determined from $c\bar{c}$ MC. We assume that this background produces negative and positive flavor tags with equal probability.

The choice of oscillated or non-oscillated VPDL *pdf* for Eq. 11 is made using the relative charge of the muon from the B_s^0 meson with respect to the sign of d_{pr} :

$$\begin{aligned} d_{pr} \cdot q_\mu > 0 : P^{x^M}(x^M, \sigma_{x^M}, d_{pr}) &= P_{\mu D_s}^{osc}(x^M, \sigma_{x^M}, d_{pr}), \\ d_{pr} \cdot q_\mu < 0 : P^{x^M}(x^M, \sigma_{x^M}, d_{pr}) &= P_{\mu D_s}^{nos}(x^M, \sigma_{x^M}, d_{pr}). \end{aligned} \quad (27)$$

The functions $D_j(K)$ and $Eff_j(x)$ were taken from Monte Carlo simulation, as explained later. The lifetimes of the B^+ and B_d^0 mesons were taken from PDG while the B_s^0 lifetime was measured using the total tagged $\mu^+ D_s^-$ sample.

B. *pdf* for the μD^- Components

As noted in Sec. IIIB there are two $\mu^+ D^-$ components present in the $m(K_S^0 K)$ spectrum, $D^- \rightarrow K_S^0 \pi^-$ and $D^- \rightarrow K_S^0 K^-$. We use Eqns. 21 and 20 to model the B_d components and Eqns. 19 and 20 to model the B_u components of these decays.

C. *pdf* for the $\mu \Lambda_c^-$ Component

We use Eqns. 28 and 29 to model the Λ_c component:

$$p_\Lambda^{nos}(x, K, d_{pr}) = \frac{K}{c\tau_\Lambda} \exp\left(-\frac{Kx}{c\tau_\Lambda}\right) \cdot 0.5 \cdot (1 - \mathcal{D}(d_{pr})), \quad (28)$$

$$p_\Lambda^{osc}(x, K, d_{pr}) = \frac{K}{c\tau_\Lambda} \exp\left(-\frac{Kx}{c\tau_\Lambda}\right) \cdot 0.5 \cdot (1 + \mathcal{D}(d_{pr})), \quad (29)$$

where τ_Λ is the lifetime of the Λ_b baryon.

D. *Pdf* for the Combinatorial Background

The following contributions to the combinatorial background were considered:

1. Quasi-vertices distributed around the primary vertex - described as a Gaussian with width $\sigma_{peak.bg}$; fraction in the background: $\mathcal{F}_{peak.bg}$.
2. A negative exponential to account for outliers in the negative x^M tail - fraction in the background: $(1 - \mathcal{F}_{peak.bg}) \cdot (1 - \mathcal{F}_{mix}) \cdot \mathcal{F}_{neg}$.
3. A long-lived background insensitive to tagging - described as an exponential with decay length $c\tau_{bg}$ convoluted with the resolution containing a background scale factor s_{bg} ; fraction in the background $(1 - \mathcal{F}_{peak.bg}) \cdot (1 - \mathcal{F}_{mix}) \cdot (1 - \mathcal{F}_{neg})$.
4. A non-oscillating long-lived background sensitive to tagging - described similarly to the insensitive long-lived background except for the multiplication of the dilution factor $1 \pm \mathcal{D}$; fraction in the background $(1 - \mathcal{F}_{peak.bg}) \cdot \mathcal{F}_{mix} \cdot (1 - \mathcal{F}_{Bd})$.
5. A long-lived background sensitive to tagging and oscillating at the frequency Δm_d - described similarly to the non-oscillating tag-sensitive background except for the multiplication of $\cos(\Delta m_d x/c)$; fraction in the background $(1 - \mathcal{F}_{peak.bg}) \cdot \mathcal{F}_{mix} \cdot \mathcal{F}_{Bd}$.

The fractions of these contributions and their parameters were determined from fitting for the B_s lifetime in the data sample. The background *pdf* is expressed in the following form:

$$P_{bg}(x^M, \sigma_{x^M}, d_{pr}) = \mathcal{F}_{peak.bg} G(0 - x^M, \sigma_{peak.bg}) + (1 - \mathcal{F}_{peak.bg}) P_{bg}^{res}(x^M, \sigma_{x^M}, d_{pr}), \quad (30)$$

$$P_{bg}^{res}(x^M, \sigma_{x^M}, d_{pr}) = (1 - \mathcal{F}_{mix}) P_{\pm} + \mathcal{F}_{mix} (\mathcal{F}_{Bd} P_{Bd} + (1 - \mathcal{F}_{Bd}) P_{Bu}), \quad (31)$$

$$P_{\pm}(x^M, \sigma_{x^M}, d_{pr}) = \mathcal{F}_{neg} \cdot \frac{-1}{c\tau_{neg}} \exp\left(-\frac{x^M}{c\tau_{neg}}\right) + (1 - \mathcal{F}_{neg}) \frac{\epsilon(x^M)}{N} \int_0^{\infty} dx \frac{1}{c\tau_{bg}} \exp\left(-\frac{x}{c\tau_{bg}}\right) \cdot G(x - x^M, s_{bg}\sigma_{x^M}), \quad (32)$$

$$P_{Bu}^{osc,nonosc}(x^M, \sigma_{x^M}, d_{pr}) = \frac{\epsilon(x^M)}{N} \int_0^{\infty} dx \frac{1}{c\tau_{bg}} \exp\left(-\frac{x}{c\tau_{bg}}\right) (1 \pm \mathcal{D}) \cdot G(x - x^M, s_{bg}\sigma_{x^M}), \quad (33)$$

$$P_{Bd}^{osc,nonosc}(x^M, \sigma_{x^M}, d_{pr}) = \frac{\epsilon(x^M)}{N} \int_0^{\infty} dx \frac{1}{c\tau_{bg}} \exp\left(-\frac{x}{c\tau_{bg}}\right) (1 \pm \mathcal{D} \cos(\Delta m_d x/c)) \cdot G(x - x^M, s_{bg}\sigma_{x^M}), \quad (34)$$

where N is the normalization constant and the fit parameters are $\mathcal{F}_{peak.bg}$, $\sigma_{peak.bg}$, \mathcal{F}_{mix} , \mathcal{F}_{Bd} , \mathcal{F}_{Bu} , τ_{bg} , τ_{neg} , and s_{bg} . The efficiency for the $B_d^0 \rightarrow D^- \mu^+ \nu X$ channel was used for $\epsilon(x^M)$.

VII. FIT INPUTS

We have used the following measured parameters for B mesons from the PDG [3] as inputs for the oscillation fitting procedure: $c\tau_{B^+} = 501 \mu\text{m}$, $c\tau_{B_d^0} = 460 \mu\text{m}$, and $\Delta m_d = 0.502 \text{ ps}^{-1}$. The latest PDG values were also used to determine the branching fractions of decays contributing to the D_s^- sample. We used the event generator EvtGen [14] since this code was developed specifically for the simulation of B decays. For those branching fractions not given in the PDG, we used the values provided by EvtGen, which are motivated by theoretical considerations. Taking into account the corresponding branching rates and reconstruction efficiencies, we calculated the contributions to our signal region from the various processes. The $B_s^0 \rightarrow D_s^- \mu^+ \nu X$ modes (including decays via D_s^{*-} , D_{s0}^{*-} , and $D_{s1}^{\prime-}$ and μ^+ originating

from τ decays) comprise $(85.3 \pm 4.5)\%$ of our sample, including reconstruction efficiency. Other backgrounds with both a real D_s^- and μ^+ and showing up in the peak, but not expected to oscillate with Δm_s , that are considered are $B \rightarrow D_{(s)}^+ D_s^- X$ decays followed by $D_{(s)}^+ \rightarrow \mu^+ \nu X$. The assigned uncertainty to each channel covers possible trigger efficiency biases. The efficiency of the lifetime selections for the sample are then determined as a function of VPDL, as shown in Fig. 4 for the decay $B_s^0 \rightarrow D_s^- \mu^+ \nu X$.

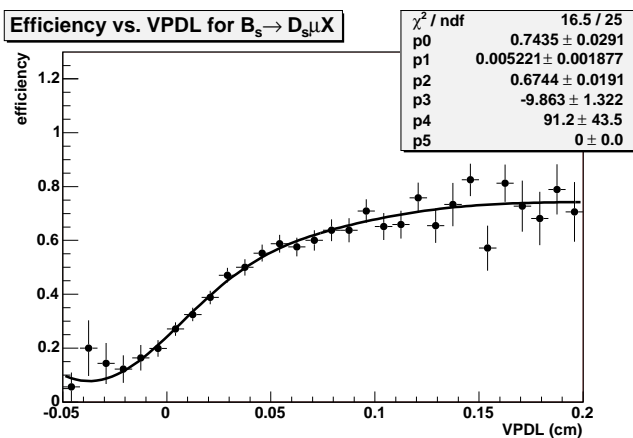


FIG. 4: Efficiency of the lifetime-dependent cuts as a function of VPDL for $B_s^0 \rightarrow D_s^- \mu^+ \nu X$.

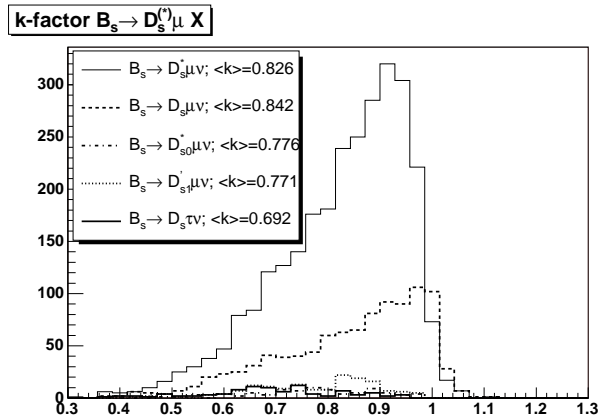


FIG. 5: K factor distributions for $B_s^0 \rightarrow \mu^+ \nu D_s^-$; $B_s^0 \rightarrow \mu^+ \nu D_s^{*-}$; $B_s^0 \rightarrow \mu^+ \nu D_{s0}^{*-}$; $B_s^0 \rightarrow \mu^+ \nu D_s^{*-}$; $B_s^0 \rightarrow \mu^+ \nu D_{s1}^-$ processes.

In determining the K factor distributions, MC generator-level information was used for the computation of p_T . Following the definition used in Eq. 10, the K factor distributions for all considered decays were determined. Figure 5 shows the distributions of the K factors for the semi-muonic decays of the B_s^0 meson. As expected, the K factors for D_s^{*-} , D_{s0}^{*-} and D_{s1}^- have lower mean values because more decay products are lost. Note that since the K factors in Eq. 10 were defined as the ratio of transverse momenta, they can exceed unity.

The total tagged sample in the entire mass range $1.4 < m(K_s^0 K) < 2.4$ GeV/ c^2 was used to determine the parameters: $\mathcal{F}_{peak.bg} = 0.022 \pm 0.007$, $\mathcal{F}_{mix} = 0.609 \pm 0.045$, $\mathcal{F}_{B_d} = 0.462 \pm 0.057$, $\mathcal{F}_{neg} = 0.0022 \pm 0.005$, $s_{bg} = 2.51 \pm 0.06$, $c\tau_{neg} = -72 \pm 30$ μm , $c\tau_{bg} = 771 \pm 8$ μm , $c\tau_{B_s} = 498 \pm 39$ μm . The discrepancy of this fitted value of $c\tau_{B_s}$ from the world average value was included as a systematic uncertainty.

A. Resolution Scale Factor

The VPDL uncertainty was estimated from the vertex fitting procedure. A resolution scale factor was introduced to take into account a possible bias. We determined this scale factor using a sample of prompt $D^{*+} \rightarrow D^0 \pi^+$ where $D^0 \rightarrow K_S^0 \pi^- \mu^+ X$. This decay has the advantage of providing a simple method for estimating the combinatorial background through the charge correlation of the two pions. The mass distributions for both charge correlations of $q(\pi) \times q(\pi_{slow})$ are shown in Fig. 6. Figure 7 shows the background-subtracted pull distribution, $PDL(D^*)/\sigma_{PDL}(D^*)$. The negative tail of the pull of distribution of the D^* vertex position with respect to the primary vertex should be a Gaussian with a sigma of unity if uncertainties assigned to the vertex position are correct. We ignore the positive side of the pull distribution as that can be biased to larger values due to D^* mesons from real B meson decays. For this study we exclude all tracks in the $D^{*+} \rightarrow D^0 \pi^+$, $D^0 \rightarrow K_S^0 \pi^- \mu^+ X$ decay chain from the primary vertex. The resulting pull distribution was fitted using a double Gaussian: the narrow Gaussian with width $\sigma_{narrow} = 0.966$ comprises 85% of the events and the wide Gaussian with width $\sigma_{wide} = 2.48$ comprises 15%.

It is known that the scale factor depends on the track transverse momenta. We took this dependence into account using the scale factor determined for D^* decays where the muon has $p_T(\mu) > 6$ GeV/ c to estimate the contribution to the systematic uncertainty. The corresponding scale factor was not different, within errors, from the default scale factor.

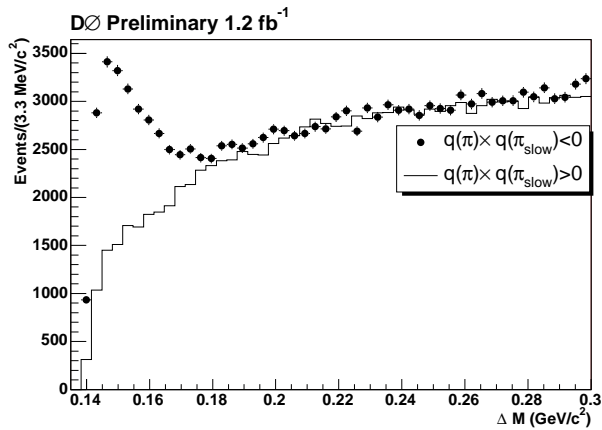


FIG. 6: Distributions of $\Delta M = m(D^*) - m(D^0)$ for $D^{*+} \rightarrow D^0 \pi^+$, $D^0 \rightarrow K_S^0 \pi^- \mu^+ X$ events. Both charge correlations of $q(\pi) \times q(\pi_{slow})$, where π refers to the pion from the D^0 and π_{slow} refers to the pion from the D^* , are shown.

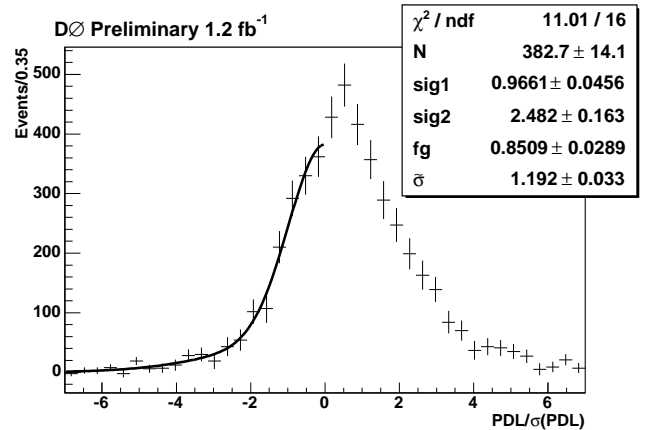


FIG. 7: A double Gaussian fit to the negative part of background subtracted $PDL(D^*)/\sigma_{PDL}(D^*)$ distributions.

VIII. AMPLITUDE FIT METHOD

The amplitude fit method [15] is a technique that can be used to calculate an experimental Δm_s oscillation limit. This technique requires a modification of Eqs. 14 and 15, yielding the form

$$p_s^{nos/osc}(x, K, d_{pr}) = \frac{K}{c\tau_{B_s^0}} \exp\left(-\frac{Kx}{c\tau_{B_s^0}}\right) \cdot 0.5 \cdot (1 \pm \mathcal{D}(d_{pr}) \cos(\Delta m_s \cdot Kx/c) \cdot \mathcal{A}), \quad (35)$$

where \mathcal{A} is now the only fit parameter.

The values of Δm_s were varied from 0 ps^{-1} to 5 ps^{-1} with a step size of 0.25 ps^{-1} . By plotting the fitted value of \mathcal{A} as a function of the input value of Δm_s , one searches for a peak of $\mathcal{A} = 1$ to obtain a measurement of Δm_s . For any value of Δm_s not equal to the “true” value of B_s^0 oscillation frequency, the amplitude \mathcal{A} should be zero. If no peak is found, limits can be set on Δm_s using this method. The expected limit (i.e., sensitivity) of a measurement is determined by calculating the probability that for a non-“true” value of Δm_s the amplitude could fluctuate to $\mathcal{A}=1$. This occurs at the lowest value of Δm_s for which $1.645 \sigma_{\mathcal{A}} = 1$ for a 95% CL, where $\sigma_{\mathcal{A}}$ is the uncertainty on the value of \mathcal{A} at the point Δm_s . The limit is determined by calculating the probability that a fitted value of \mathcal{A} could fluctuate to $\mathcal{A} = 1$. This occurs at the lowest value of Δm_s for which $\mathcal{A} + 1.645\sigma_{\mathcal{A}} = 1$.

Figure 8 shows the dependence of the parameter \mathcal{A} from Eq. 35, and its uncertainty, on Δm_s . In the figure, the yellow (light shaded) and green (dark shaded) regions indicate 1.645 times the statistical uncertainty and 1.645 times the statistical plus systematic uncertainties, respectively. A 95% confidence level limit on the oscillation frequency $\Delta m_s > 1.15 \text{ ps}^{-1}$ and sensitivity of 2.19 ps^{-1} were obtained with statistical uncertainties only.

IX. SYSTEMATIC UNCERTAINTIES

All studied contributions to the systematic uncertainty of the amplitude are listed in Table I. For each Δm_s step, the deviations of $\Delta \mathcal{A}$ and $\Delta \sigma_{\mathcal{A}}$ from the default values are given. One can see that the largest deviations come from the uncertainty in the signal yield. The resulting systematic uncertainties were obtained using the formula from Ref. [15]:

$$\sigma_{\mathcal{A}}^{sys} = \Delta \mathcal{A} + (1 - \mathcal{A}) \frac{\Delta \sigma_{\mathcal{A}}}{\sigma_{\mathcal{A}}}, \quad (36)$$

and were summed in quadrature. The effect of the systematic uncertainties is represented by the green (dark shaded) region in Fig. 8. Taking into account the systematic uncertainties, we obtained a 95% confidence level limit on the oscillation frequency $\Delta m_s > 1.09 \text{ ps}^{-1}$ and an expected limit of 1.90 ps^{-1} .

The decays $B_s^0 \rightarrow X \mu^+ D^- (\rightarrow K_S^0 \pi \text{ and } K_S^0 K)$ as well as the background component oscillating at Δm_d allow a cross-check of the entire fitting procedure using B_d^0 decays present in the same data sample as the signal $B_s^0 \rightarrow D_s^- \mu^+ X$,

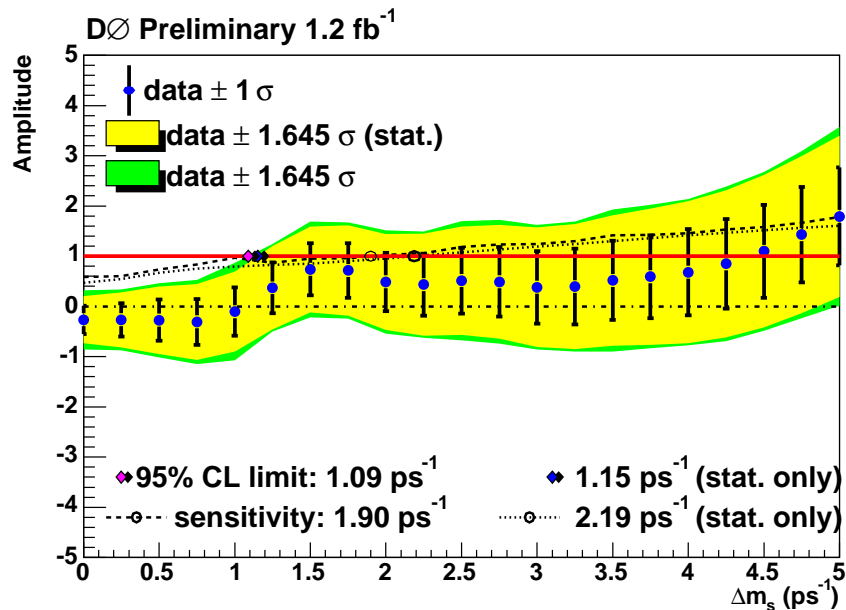


FIG. 8: B_s^0 oscillation amplitude with statistical and systematic errors.

$D_s^- \rightarrow K_S^0 K^-$ events. Figure 9 shows the dependence of the parameter \mathcal{A} and its uncertainty on the B_d^0 oscillation frequency, Δm_d , which has a world-average value of $\Delta m_d = 0.502 \pm 0.007 \text{ ps}^{-1}$ [3]. The peak in the amplitude scan at $\Delta m_d \approx 0.5 \text{ ps}^{-1}$ reveals the oscillations in the $B_d^0 - \bar{B}_d^0$ system. After transforming the scan in Fig. 9 to a likelihood referenced to infinity as described in Ref. [15], we obtain $\Delta m_s = 0.50 \pm 0.13$, in agreement with the world average [3]. This confirms that the dilution calibration is correct.

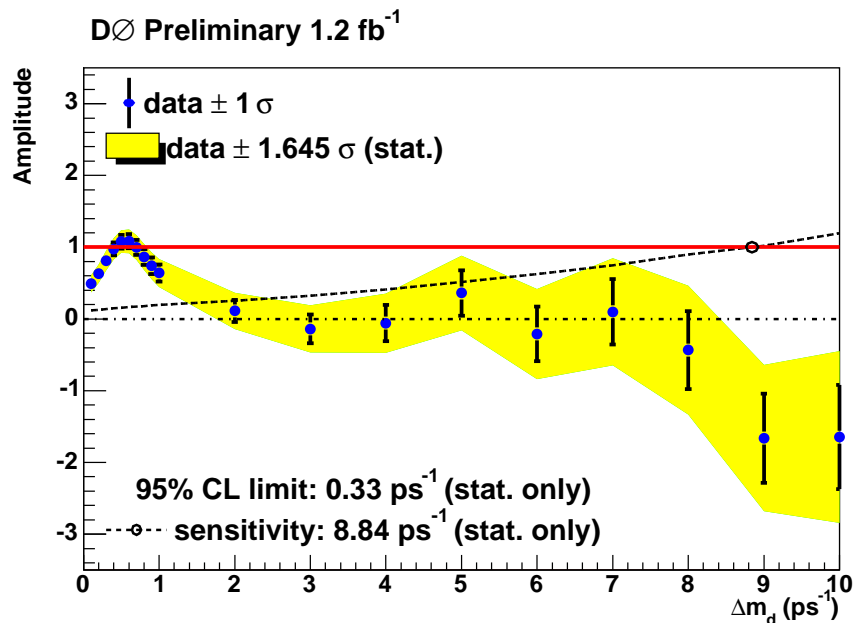


FIG. 9: The $B_d^0 - \bar{B}_d^0$ oscillation amplitude scanning the $D^- \rightarrow K_S^0 \pi^-$, $D^- \rightarrow K_S^0 K^-$, and combinatorial Δm_d -oscillating background components.

TABLE I: Systematic uncertainties on the amplitude. The shifts of both the measured amplitude, $\Delta\mathcal{A}$, and its statistical uncertainty, $\Delta\sigma$, are listed

Osc. frequency (ps^{-1})		0.00	0.50	1.00	1.50	2.00	2.50	3.00	3.50	4.00	4.50	5.00
\mathcal{A}		-0.284	-0.282	-0.188	0.771	0.432	0.539	0.358	0.543	0.668	1.130	1.934
Stat. uncertainty		0.281	0.420	0.489	0.528	0.595	0.678	0.754	0.829	0.908	0.980	1.036
Dilution	$\Delta\mathcal{A}$	-0.013	-0.034	-0.006	-0.022	+0.002	+0.002	-0.003	+0.008	+0.049	+0.069	+0.085
	$\Delta\sigma$	-0.002	-0.003	-0.004	-0.003	-0.003	-0.004	-0.005	-0.008	-0.009	-0.009	-0.010
Scale Factor	$\Delta\mathcal{A}$	-0.002	+0.009	+0.027	+0.024	+0.007	-0.014	-0.029	-0.038	-0.038	-0.030	-0.018
	$\Delta\sigma$	-0.000	+0.000	-0.000	-0.000	-0.000	-0.001	-0.002	-0.004	-0.003	-0.002	-0.000
$Br(B_s \rightarrow D_s \mu \nu) = 5.5\%$	$\Delta\mathcal{A}$	+0.014	+0.018	-0.002	+0.020	+0.011	+0.014	+0.009	+0.017	+0.021	+0.039	+0.069
	$\Delta\sigma$	+0.010	+0.015	+0.019	+0.020	+0.023	+0.026	+0.030	+0.033	+0.036	+0.039	+0.041
$Br(B_s \rightarrow D_s D_s) = 5.5\%$	$\Delta\mathcal{A}$	+0.012	+0.016	-0.003	+0.024	+0.014	+0.017	+0.011	+0.020	+0.025	+0.044	+0.079
	$\Delta\sigma$	+0.012	+0.018	+0.021	+0.023	+0.026	+0.030	+0.033	+0.037	+0.040	+0.044	+0.047
$Br(B_s \rightarrow D_s D_s) = 23\%$	$\Delta\mathcal{A}$	-0.008	-0.009	-0.003	+0.014	+0.010	+0.010	+0.007	+0.009	+0.012	+0.020	+0.034
	$\Delta\sigma$	+0.005	+0.008	+0.009	+0.009	+0.010	+0.012	+0.013	+0.014	+0.016	+0.017	+0.018
$c\bar{c} : 4.62\%$	$\Delta\mathcal{A}$	-0.002	+0.001	+0.005	+0.018	+0.010	+0.007	+0.002	+0.002	+0.002	+0.007	+0.019
	$\Delta\sigma$	+0.003	+0.005	+0.006	+0.006	+0.007	+0.008	+0.009	+0.010	+0.012	+0.013	+0.014
$c\tau_{B_s} = 438\mu m$	$\Delta\mathcal{A}$	-0.016	-0.006	-0.079	+0.049	-0.049	+0.031	-0.024	+0.024	-0.014	+0.034	+0.150
	$\Delta\sigma$	-0.002	+0.014	+0.009	+0.013	+0.020	+0.028	+0.036	+0.046	+0.055	+0.065	+0.069
$p_{T_\mu} > 6 \text{ GeV}/c$	$\Delta\mathcal{A}$	-0.035	-0.032	-0.082	+0.011	-0.070	+0.011	-0.034	+0.004	-0.038	-0.013	+0.058
	$\Delta\sigma$	-0.016	-0.008	-0.017	-0.014	-0.012	-0.008	-0.005	+0.000	+0.005	+0.010	+0.011
D_s yield $\pm 1.15\sigma$	$\Delta\mathcal{A}$	+0.071	+0.121	-0.035	+0.136	+0.019	+0.115	+0.066	+0.140	+0.079	+0.151	+0.363
	$\Delta\sigma$	-0.028	-0.026	-0.037	+0.067	+0.082	+0.098	+0.117	+0.134	+0.149	+0.166	+0.176
D^+ yield $\pm 1\sigma$	$\Delta\mathcal{A}$	+0.038	+0.079	-0.043	+0.082	-0.095	+0.083	+0.027	+0.084	+0.032	+0.097	+0.267
	$\Delta\sigma$	-0.018	-0.012	-0.021	+0.040	-0.016	+0.063	+0.076	+0.089	+0.102	+0.116	+0.123
k-factor $\pm 2\%$	$\Delta\mathcal{A}$	-0.027	-0.006	-0.108	+0.038	-0.087	+0.030	+0.005	+0.046	+0.050	+0.149	+0.258
	$\Delta\sigma$	-0.003	+0.012	+0.005	+0.011	+0.020	+0.028	+0.026	+0.047	+0.055	+0.063	+0.071
k-factor smoothed	$\Delta\mathcal{A}$	-0.017	-0.009	-0.086	+0.034	-0.055	+0.032	-0.022	+0.028	-0.010	+0.046	+0.153
	$\Delta\sigma$	-0.003	+0.011	+0.006	+0.010	+0.017	+0.025	+0.032	+0.042	+0.050	+0.060	+0.064
Reco k-factor	$\Delta\mathcal{A}$	-0.018	-0.009	-0.089	+0.040	-0.031	+0.059	-0.014	+0.048	+0.045	+0.109	+0.166
	$\Delta\sigma$	-0.003	+0.012	+0.009	+0.015	+0.024	+0.034	+0.044	+0.057	+0.068	+0.079	+0.086
BG Scale Factor = 2.0	$\Delta\mathcal{A}$	-0.018	-0.021	-0.109	+0.030	-0.062	+0.026	-0.028	+0.018	-0.021	+0.027	+0.139
	$\Delta\sigma$	-0.003	+0.015	+0.008	+0.012	+0.018	+0.026	+0.034	+0.044	+0.052	+0.061	+0.065
$frNeg + 1\sigma$	$\Delta\mathcal{A}$	-0.017	-0.010	-0.086	+0.035	-0.056	+0.028	-0.022	+0.026	-0.012	+0.035	+0.143
	$\Delta\sigma$	-0.004	+0.011	+0.006	+0.010	+0.016	+0.023	+0.031	+0.040	+0.048	+0.057	+0.061
$f_{cc}(bg) \pm 1\sigma$	$\Delta\mathcal{A}$	-0.021	-0.003	-0.090	+0.040	-0.063	+0.034	-0.019	+0.027	-0.012	+0.035	+0.144
	$\Delta\sigma$	-0.003	+0.011	+0.006	+0.010	+0.016	+0.023	+0.031	+0.040	+0.048	+0.057	+0.061
frBd $\pm 1\sigma$	$\Delta\mathcal{A}$	-0.060	-0.007	-0.115	+0.045	-0.060	+0.029	-0.022	+0.026	-0.011	+0.034	+0.142
	$\Delta\sigma$	-0.003	+0.012	+0.006	+0.009	+0.016	+0.023	+0.031	+0.041	+0.048	+0.057	+0.060
frMix $\pm 1\sigma$	$\Delta\mathcal{A}$	-0.067	+0.059	-0.111	+0.041	-0.076	+0.048	-0.006	+0.038	-0.001	+0.044	+0.150
	$\Delta\sigma$	-0.003	+0.011	+0.005	+0.009	+0.017	+0.022	+0.029	+0.038	+0.046	+0.055	+0.059
Background Mass Shape	$\Delta\mathcal{A}$	-0.034	-0.023	-0.064	+0.030	-0.047	+0.016	-0.021	+0.053	+0.020	+0.030	+0.100
	$\Delta\sigma$	+0.001	+0.015	+0.009	+0.012	+0.017	+0.031	+0.041	+0.048	+0.049	+0.050	+0.050
$N(D^+ \rightarrow K_S^0 K)/N(D^+ \rightarrow K_S^0 \pi) \pm 0.035$	$\Delta\mathcal{A}$	+0.005	+0.022	-0.076	+0.057	-0.074	+0.044	-0.009	+0.042	-0.002	+0.049	+0.178
	$\Delta\sigma$	-0.010	+0.002	-0.005	+0.021	+0.003	+0.037	+0.047	+0.058	+0.067	+0.078	+0.083
Total syst.	σ_{tot}^{sys}	0.216	0.186	0.338	0.260	0.236	0.300	0.211	0.343	0.208	0.270	0.467
Total	σ_{tot}	0.357	0.449	0.589	0.580	0.626	0.720	0.753	0.860	0.885	0.962	1.081

X. CONCLUSIONS

Using $B_s^0 \rightarrow D_s^- \mu^+ X$ decays, where $D_s^- \rightarrow K_S^0 K^-$ in combination with an opposite-side flavor tagging algorithm and an unbinned likelihood fit, we performed a search for $B_s^0 - \bar{B}_s^0$ oscillations. We obtain a 95% confidence level limit on the oscillation frequency $\Delta m_s > 1.09 \text{ ps}^{-1}$ and a sensitivity of 1.90 ps^{-1} . In Appendix A this result is combined with the other analyzed B_s^0 decay channels at DØ.

APPENDIX A: COMBINED OSCILLATION SCAN

As in Ref. [7], we use the “combos” program [16] developed at LEP to combine results, taking into account correlated errors properly. We combine the $\mu\phi\pi$, $\mu\phi e$, $\mu K^* K$, and $\mu K_S^0 K$ modes taking the following uncertainties as correlated:

- $Br(B_s \rightarrow X\mu D_s)$.
- $Br(B_s \rightarrow X D_s D_s)$.
- Signal decay length resolution for all semi-muonic modes.
- $\Delta\Gamma/\Gamma$.

Figure 10 shows the result of the combined amplitude scan. A 95% C.L. of $\Delta m_s > 14.9 \text{ ps}^{-1}$ with a corresponding expected limit of 16.5 ps^{-1} are obtained.

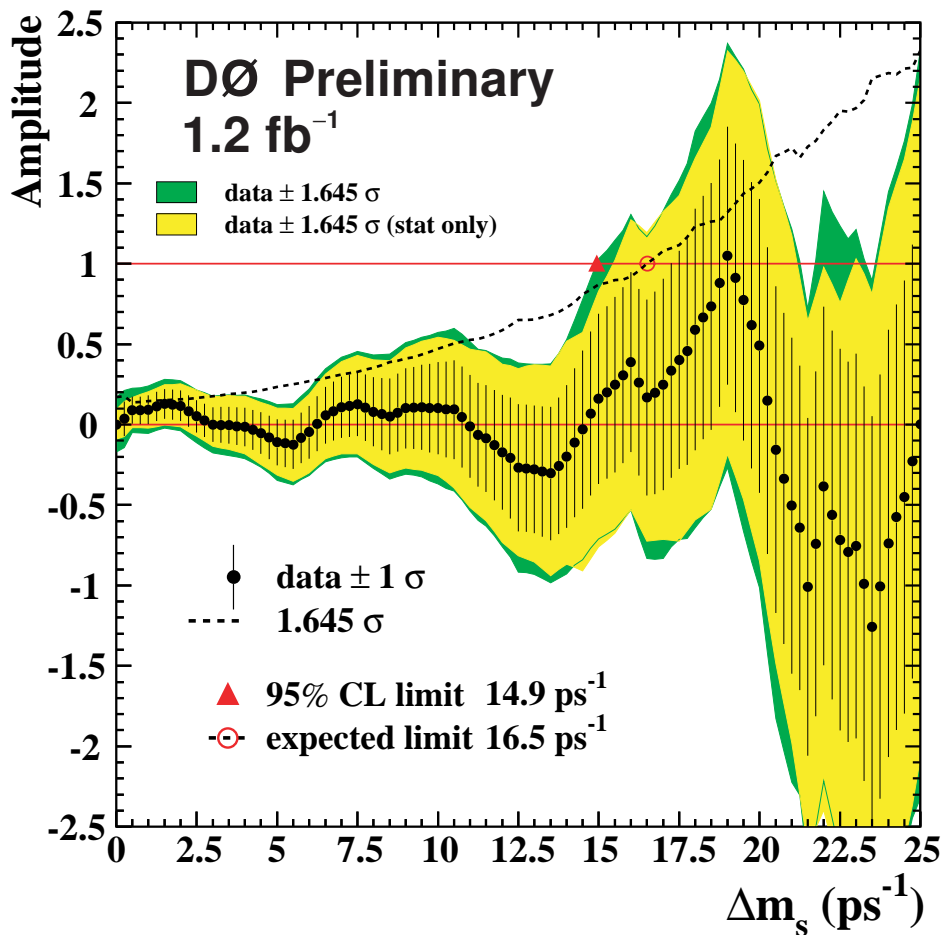


FIG. 10: B_s^0 oscillation amplitude with statistical and systematic errors for $B_s^0 \rightarrow D_s^- e^+ X$ ($D_s^- \rightarrow \phi\pi^-$) and $B_s^0 \rightarrow D_s^- \mu^+ X$ ($D_s^- \rightarrow \phi\pi^-$ and $D_s^- \rightarrow K^* K$ and $D_s^- \rightarrow K_S^0 K^-$).

ACKNOWLEDGMENTS

We thank the staffs at Fermilab and collaborating institutions, and acknowledge support from the DOE and NSF (USA); CEA and CNRS/IN2P3 (France); FASI, Rosatom and RFBR (Russia); CAPES, CNPq, FAPERJ, FAPESP and FUNDUNESP (Brazil); DAE and DST (India); Colciencias (Colombia); CONACyT (Mexico); KRF and KOSEF (Korea); CONICET and UBACyT (Argentina); FOM (The Netherlands); PPARC (United Kingdom); MSMT (Czech Republic); CRC Program, CFI, NSERC and WestGrid Project (Canada); BMBF and DFG (Germany); SFI (Ireland); Research Corporation, Alexander von Humboldt Foundation, and the Marie Curie Program.

-
- [1] UA1 Collaboration, C. Albajar *et al.*, Phys. Lett. **B186**, 247 (1987).
 - [2] ARGUS Collaboration, H. Albrecht *et al.*, Phys. Lett. **B192**, 245 (1987).
 - [3] S. Eidelman *et al.*, Phys. Lett. **B592**, 1 (2004).
 - [4] K. Anikeev *et al.*, *B* Physics at the Tevatron: Run II and Beyond, arxiv:hep-ph/0201071.
 - [5] DØ Collaboration, V.M. Abazov *et al.*, Phys. Rev. Lett. **97**, 21802 (2006).
 - [6] CDF Collaboration, A. Abulencia *et al.*, *Measurement of B_s^0 -Anti- B_s^0 Oscillation Frequency*, Submitted in Physical Review Letters, arXiv:hep-ex/0606027.
 - [7] G. Borissov *et al.*, *DØ Note 5207*, Combination of B_s Oscillation Results from DØ.
 - [8] DØ Collaboration, V.M. Abazov *et al.*, Nucl. Instrum. Methods Phys. Res. A **565**, 463-537 (2006).
 - [9] S. Catani, Yu.L. Dokshitzer, M. Olsson, G. Turnock, B.R. Webber, Phys. Lett. **B269** 432 (1991).
 - [10] T. Sjöstrand *et al.*, hep-ph/0108264.
 - [11] G. Borisov, Nucl. Instrum. Methods Phys. Res. A **417**, 384 (1998).
 - [12] DØ Collaboration, V.M. Abazov *et al.*, *Measurement of B_d mixing using opposite-side flavor tagging*, submitted to Physical Review D, arXiv:hep-ex/0609034v1.
 - [13] F. James, MINUIT - Function Minimization and Error Analysis, CERN Program Library Long Writeup D506 (1998).
 - [14] D.J. Lange, Nucl. Instrum. Methods Phys. Res. A **462**, 152 (2001); for details see <http://www.slac.stanford.edu/~lange/EvtGen>.
 - [15] H.G. Moser and A. Roussarie, Nucl. Instrum. Methods Phys. Res. A **384**, 491 (1997).
 - [16] <http://lepbose.web.cern.ch/LEPBOSC/combos/>.